

# Wideband Radar Cross Section Reduction of Microstrip Patch Antenna using Polarization Converter Metasurface

Krunal Patel,\* and Manjusha Joshi

MPSTME, NMIMS University, Mumbai, Maharashtra – 400 056, India

\*E-mail: krunalmailbox@rediffmail.com

## ABSTRACT

An antenna is the key device of communication on a stealth platform. It is the greatest contributor to the overall Radar Cross Section (RCS). So, it is desired to reduce the radar signature of the antenna. In this paper, a novel antenna is designed using a polarization converter metasurface. The polarization converter metasurface converts the polarization of the incident wave into its orthogonal component. This Polarization Converter Metasurface (PCM) is loaded around the patch antenna to reduce the RCS of the antenna over a wide frequency range. With this novel design, the overall Radar Cross Section reduction bandwidth of 140.57 % is obtained for the frequency range of 3.49 GHz – 20 GHz. In addition to this, the 10 dB RCS reduction bandwidth is obtained for the frequency ranges of 8.84 GHz – 10.42 GHz (16.41 %) and 16.99 GHz – 17.81 GHz (4.71 %). The design shows excellent angular stability for both Transverse Electric and Transverse Magnetic polarization. Discernible Bistatic RCS reduction is obtained over a wide frequency range. Simulation and experimental results show that there is no degradation of antenna radiation pattern and other parameters. So, with this novel design, the problem of obtaining wideband RCS reduction of a microstrip patch antenna is addressed without degradation in radiation pattern along with excellent angular stability for both the polarization modes.

**Keywords:** Radar cross section reduction; Microstrip patch antenna; Polarization converter metasurface; Antenna radiation pattern

## 1. INTRODUCTION

Metasurfaces have powerful capabilities of manipulating the reflection phase of the incident wave, changing the polarization state, modifying the permittivity and permeability of the material and absorption of electromagnetic waves. Due to the excellent properties of metamaterials and metasurfaces, they can be used for various applications like gain enhancement of antennas<sup>1,2</sup> and Radar Cross Section reduction (RCS).<sup>3-4,24</sup> Metasurfaces take less space than bulky metamaterial structures, so they are suitable for planar structures. An antenna is used for communication on the military platforms. However, it contributes significantly to the overall RCS. Traditional methods of using Radar Absorbing Materials<sup>5</sup> degrade the antenna radiation pattern. The Radar Absorbing Materials are not suitable for the aerodynamic shape of the weapon. Metamaterial absorbers with shielded rear sides have been reported.<sup>6-7</sup> An MTM absorber was used to achieve RCS reduction, but the device exhibited narrow band performance.<sup>8</sup>

The RCS reduction bandwidth was from 7 GHz to 12.8 GHz. The percentage bandwidth was 58.59 %. A Spiral Coding Metasurface<sup>9</sup> was used to achieve RCS reduction. The metasurface exhibited low RCS reduction bandwidth. It offered percentage bandwidth of 62.92 % (13.2 GHz-23 GHz). The surface was not integrated with the patch antenna. Wen Jiang<sup>10</sup> represented an oblique Split Ring Resonator for RCS reduction. Percentage bandwidth of 61.69 % in the frequency

range of 10.2-19.3 GHz was achieved with this methodology. The design was not integrated with the patch antenna. Wideband polarization converters were designed but they did not obtain polarization conversion for oblique incidence.<sup>11-12</sup> Yang<sup>13</sup> reported a Polarization Converter Metamaterial based on square loop-shaped structures<sup>25</sup> which achieved polarization conversion from 5.50-8.94 GHz and 13.30-15.50 GHz for linear polarization. The percentage bandwidth was 47.75 % and 16.78 % respectively. The polarization conversion ratio was larger than 0.90 in the frequency ranges of 5.70-8.62 GHz and 13.30-15.50 GHz. The structure was not used for RCS reduction of a patch antenna. Polarization conversion can also be achieved by the Faraday Effect and birefringent crystals<sup>14-15</sup>. These methods are traditional and show limited bandwidth. The polarization converters designed using these methods are bulky and not suitable for microstrip antennas.

Qi,<sup>16</sup> *et al.* used an anisotropic Double Split Ring Resonator structure to design a polarization converter. The proposed structure obtained good polarization conversion in a frequency range of 2.04 THz to 5.33 THz with a relative bandwidth of 89 %. In order to address the problem of RCS reduction of patch antenna over a wider bandwidth while maintaining excellent performance and angular stability, metasurfaces can be used for coplanar loading. The Polarization Converter Metasurfaces (PCMs)<sup>20-22,26</sup> provide excellent RCS reduction. PCM structures can be used in receiving mode to manipulate the reflection phase of the incident wave. In this paper, a novel metasurface is designed by the author and its RCS reduction characteristics are studied. Then the metasurface is used to

design a novel patch antenna which shows RCS reduction over a wide bandwidth. In the published literature, narrowband RCS reduction is observed and the obtained RCS reduction is not significant when the metasurface is integrated with the patch antenna. The main novelty of the proposed design is its wideband RCS reduction performance without degradation in antenna radiation pattern and other parameters and its angular stability.

**2. DESIGN OF POLARIZATION CONVERTER METASURFACE**

Conventional SRR geometry is modified to design the polarization converter. In the modified design two additional gaps are created. One split is created in the outer SRR and the other split is created in the inner SRR. Both the splits are located on the opposite sides. If the wave is incident on the side without a gap, then it causes the current flow only in that side. If the wave is incident on the side with the gap, then it can also cause the current flow in the side without a gap which

is perpendicular to the former. The electric currents in both these types of sides have a phase difference. So at resonance frequencies, the net current flow is maximized in the direction which is perpendicular to the polarization of the incident wave. With this type of design, an incident x-polarized wave is converted into a y-polarized wave after reflection from the metasurface. So, the metasurface is known as ‘Polarization Converter Metasurface’. This is not possible when a single split is used or both the splits are not created on the opposite sides. The dimensions are optimized in Ansys HFSS software to obtain the required cross-polarization conversion. Figure 1(a) shows the geometry of the conventional SRR and Fig. 1(b) shows the geometry of the modified SRR. To simulate the polarization converter metasurface Master-Slave boundary conditions are used and Floquet ports are defined with de-embedding.

The PCM structure is designed on an FR-4 substrate with the height of 2.4 mm. The relative permittivity of the substrate is 4.3 and the dielectric loss tangent is 0.02. The optimized

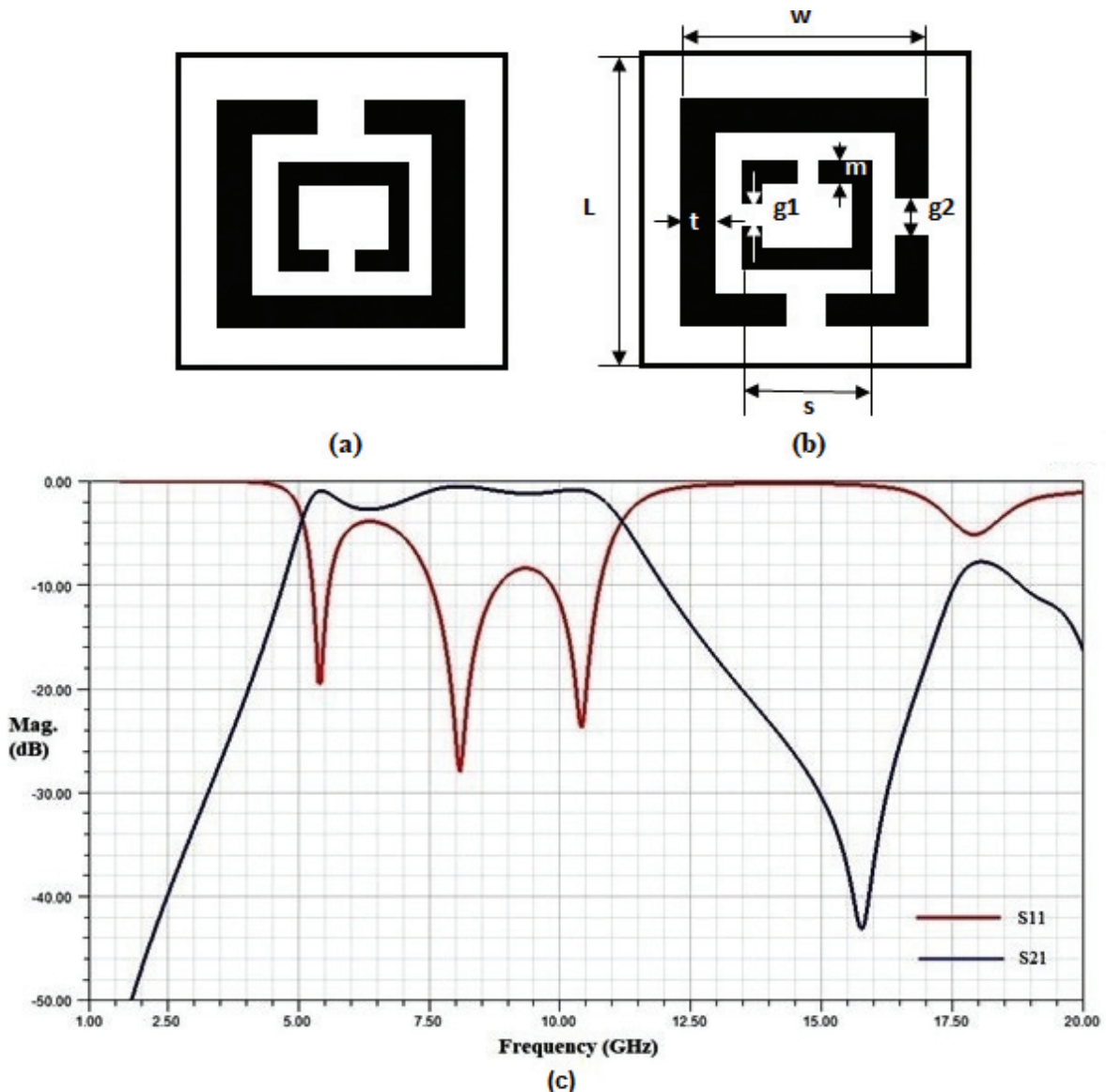


Figure 1. (a) Conventional SRR geometry, (b) Modified SRR geometry and (c) Co-polarized and cross-polarized reflection coefficients.

dimensions in mm are as follows:  $L=7$ ,  $W=6$ ,  $t=1$ ,  $m=0.5$ ,  $g_1=0.5$ ,  $s=3$  and  $g_2=1$  mm. The Copper layer has a thickness of 35 microns.

The simulated co-polar reflection ( $S_{11}$ ) and cross-polar reflection coefficients ( $S_{21}$ ) are shown in Fig. 1 (c). It is clear from Fig. 1 (c) that the co-polarized reflection is minimized at the frequencies of 5.25 GHz, 8.02 GHz, 10.85 GHz and 17.52 GHz. The values of co-polarized reflection coefficients are -20.52 dB, -27.56 dB, -24.72 dB and -5.28 dB respectively. These frequencies are identified as resonant frequencies. The overall co-polarized reduction is observed from 4.2 GHz to 12 GHz and from 16.25 GHz to 19 GHz. As shown in Fig. 1(c), the cross-polarized reflection coefficient is increased for this frequency range. At resonant frequencies, the cross-polarized reflection is maximized. From the knowledge of surface current distribution, the direction of the reflected field can be determined.

The polarization conversion ratio is defined as<sup>12</sup>

$$PCR = \frac{|\Gamma_{yx}|^2}{|\Gamma_{yx}|^2 + |\Gamma_{xx}|^2} \quad (1)$$

$\Gamma_{yx}$  indicates the reflection coefficient when the reflected

field is in the y-direction and the incident field is in the x-direction. Similarly,  $\Gamma_{xx}$  indicates the reflection coefficient when the reflected field is in the x-direction and the incident field is in the x-direction. The values of the Polarization Conversion Ratio (PCR) are approaching unity at the resonance frequencies of 5.25 GHz, 8.02 GHz and 10.85 GHz. At these frequencies, excellent cross-polarization conversion can be achieved.

### 2.1 Angular Stability

The metasurface should exhibit angularly stable performance because often the direction of the incident wave is unknown. By using the proper thickness and dielectric constant of the metasurface, the angular stability of the structure can be controlled. For better angular stability, a thinner dielectric substrate should be used<sup>27</sup>. If substrate material of higher relative permittivity is used, then angular stability can also be achieved at the cost of reduction in bandwidth. The angular stability is verified for the TE as well as TM polarization. For cross-polarized mode, angular stability is achieved due to structural symmetry and smaller dimensions of the unit cell as compared with the wavelength. As shown in Fig. 2(a), the structure shows excellent angular stability for various angles of

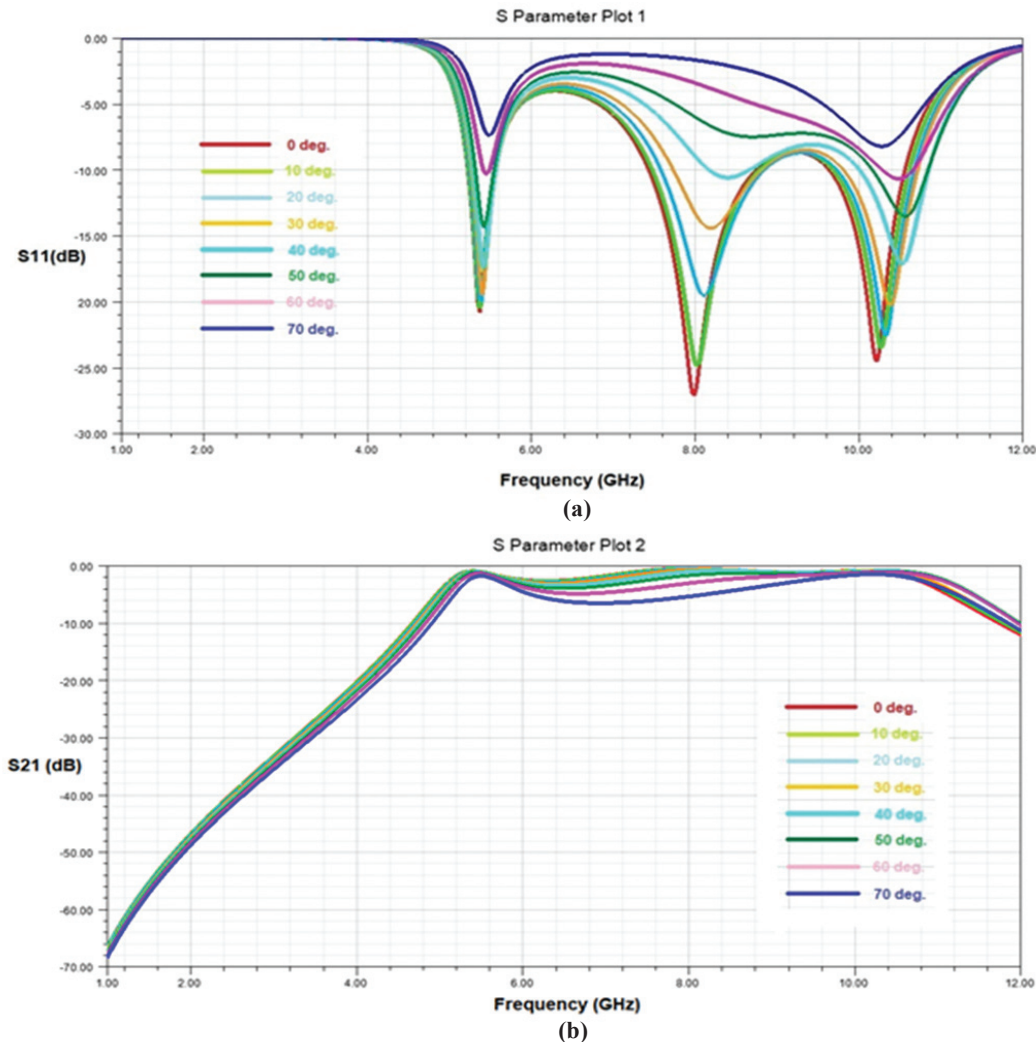


Figure 2. (a) Co-polarized reflection coefficient under various angles of incidence and (b) cross-polarized reflection coefficient under various angles of incidence.

incidence. Significant reduction of co-polar components can be obtained for the oblique incidences up to 60 deg. As shown in Fig. 2(b), the cross-polar reflection coefficient is the same for various angles of incidence. So, the design exhibits excellent angular stability up to 70 deg. oblique incidence.

**3. DESIGN OF METASURFACE**

As shown in Fig. 3 (a) and Fig. 3 (b), the incident y-polarized wave is resolved into two components. Mode 1 is considered as a V-polarized wave and Mode 2 is considered as a U-polarized wave. The resonances at 5.25 GHz, 10.85 GHz and 17.52 GHz are obtained due to the V-polarized wave and the resonance at 8.02 GHz is obtained by the U-polarized wave as shown in Fig. 3 (d). At 17.52 GHz, the magnitude of the reflection coefficient decreases. Depending upon the direction of the surface current on the top and the bottom sides of the unit cell, the type of resonance can be determined.

At the resonant frequency, if the directions of the current flowing on the surface and the current flowing on the ground plane are the same then Electric Resonance occurs and the reflected field will be out of phase by 180 deg. with the incident field. If the directions of surface current on the top side and

on the ground plane are opposite then Magnetic Resonance occurs. In this case, the reflected field will be in-phase with the incident field. The structure behaves like an AMC and as per Faraday’s law, the time-varying magnetic field will produce a curling electric field. Because of multiple resonance characteristics, wide polarization conversion bandwidth is achieved. So, at the specified frequency of resonance, if the U-polarized component is reflected in-phase then the orthogonal V-polarized component will be reflected 180 deg. out of phase. Because of vector addition, the reflected Electric Field will be x-polarized if the incident field is y-polarized as shown in Fig. 3 (c). The reflected field from the unit cells arranged in the mirror configuration will be in the opposite direction. So, by arranging the unit cells in the mirror configuration, broadband RCS reduction can be obtained because of opposite phase cancellation.

For normal incidence, the incident electric field can be written as,

$$\vec{E}_{ix} = E_u e^{i(-kz-\omega t)} a_u + E_v e^{i(-kz-\omega t)} a_v \tag{2}$$

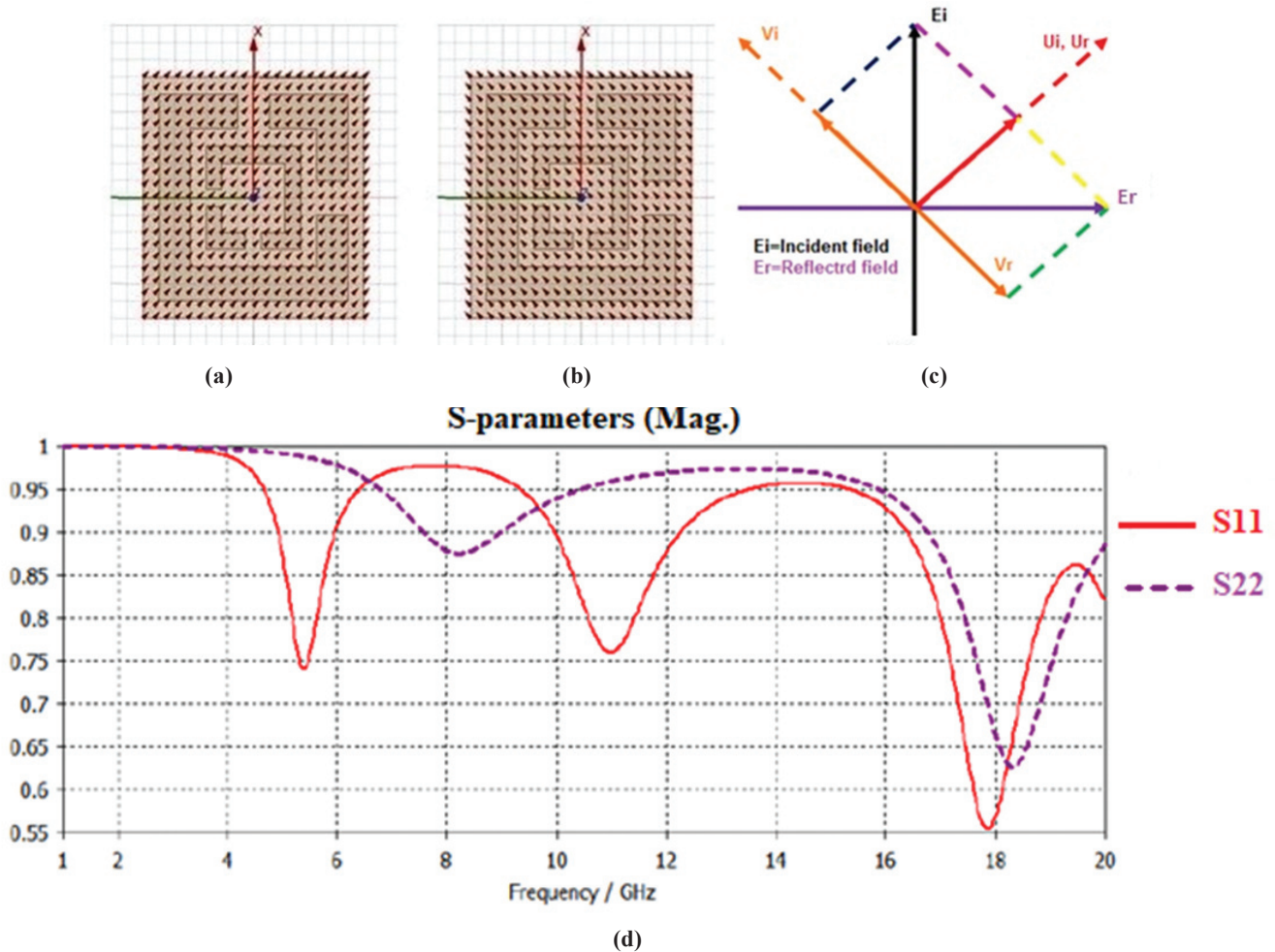


Figure 3. (a) Incident U-polarized wave, (b) Incident V-polarized wave, (c) Mechanism of polarization conversion, and (d) Reflection coefficient magnitudes of mode 1 and mode 2.

The reflected fields are given by,

$$\vec{E}_{rx} = E_u e^{i(kz - \omega t + \phi_u)} \mathbf{a}_u + E_v e^{i(kz - \omega t + \phi_v)} \mathbf{a}_v \quad (3)$$

where,  $\mathbf{a}_u$  and  $\mathbf{a}_v$  indicate the unit vectors in U and V directions respectively. To design a polarization converter metasurface for RCS reduction, four different configurations were examined as shown in Fig. 4 (a). The metasurface is divided into four regions (Regions 1 to 4). In Configuration 1 the PCM unit cells in adjacent regions are in opposite directions. In Configuration 2, the unit cells are rotated as shown in Fig. 4 (a). In configuration 3, the unit cells in the adjacent regions are arranged in the mirror configuration. In the fourth configuration, all the PCM unit cells are arranged in the same direction. The monostatic radar cross section of all the configurations is simulated in CST Microwave Studio software. It is observed that no RCS reduction is observed for Configuration 4 in which all the unit cells are in the same direction. If all the unit cells are in the same direction then reflection from all the regions of the metasurface will be in the same direction. So, opposite phase cancellation does not occur and the reflected wave is polarized in one direction only which is perpendicular to the polarization of the incident wave. Configuration 3 offers better RCS reduction as compared with other configurations. The reflected fields from the adjacent regions are out of phase by 180 deg., so reflected fields from these regions are cancelled. Because of this, maximum RCS reduction can be observed for this configuration.

The reflected electric field from Region 1 of the metasurface is given by,

$$\vec{E}_1 = A_1 e^{j\phi_1} \quad (4)$$

The reflected electric field from Region 2 of the metasurface is given by,

$$\vec{E}_2 = A_2 e^{j\phi_2} = A_1 e^{j(\phi_1 \pm 180^\circ)} \quad (5)$$

where  $A_1$ ,  $A_2$  indicate the amplitudes and  $\phi_1$ ,  $\phi_2$  indicate the Reflection Phase of the fields.

The total reflected field from the metasurface is,

$$\vec{E}_{pcm} = \vec{E}_1 + \vec{E}_2 = A_1 e^{j\phi_1} + A_1 e^{j(\phi_1 \pm 180^\circ)} \quad (6)$$

If the phase difference between the two regions is not 180 deg., then the equation can be generalized as,

$$\vec{E}_{pcm} = \vec{E}_1 + \vec{E}_2 = A_1 e^{j\phi_1} \left( 1 + e^{j(\phi_2 - \phi_1)} \right) \quad (7)$$

For a metal sheet,  $\phi_1 = \phi_2$  and the reflected field is given by,

$$\vec{E}_{metal} = 2A_1 e^{j\phi_1} \quad (8)$$

For -10 dB RCS reduction

$$\frac{|\vec{E}_{pcm}|^2}{|\vec{E}_{metal}|^2} \leq -10 \text{ dB} \quad (9)$$

Then

$$\cos(\phi_2 - \phi_1) \leq -0.8 \quad (10)$$

So, the required phase difference for -10 dB RCS reduction is,

$$143^\circ \leq |\phi_2 - \phi_1| \leq 217^\circ \quad (11)$$

Radar Cross Section  $\sigma$  is measured in dBsm and mathematically it is defined as

$$\sigma = \lim_{r \rightarrow \infty} 4\pi r^2 \frac{|E^{scat}|^2}{|E^{inc}|^2} \quad (12)$$

where,  $E^{scat}$  indicates the scattered field,  $E^{inc}$  is the field incident on the target and  $r$  is the distance between the target and the receiving antenna.

#### 4. ANTENNA DESIGN

To design the most suitable configuration of the metasurface loaded patch antenna, the following steps were required. For Configurations 1 to 4 and Simple Patch 1, the substrate and the ground plane dimensions are 56 mm × 56 mm. For Configurations 5, 6 and Simple Patch 2, the substrate and the ground plane dimensions are 70 mm × 70 mm. For all the configurations, the square patch dimensions are 18 mm × 18 mm and the substrate height is 2.4 mm. The Copper thickness is 35 microns. In Configuration 1, the metasurface unit cells are arranged in two rows and two columns as shown in Fig. 4 (b). In Configuration 2, the cells in the adjacent columns are rotated by 90 deg. and the RCS values were obtained. In Configuration 3, the cells in the adjacent rows and columns were rotated by 90 deg. and RCS simulations were carried out. In Configuration 4, all the unit cells were rotated by 180 deg. and the RCS reduction performance was compared.

In Configuration 5, more unit cells are added and the unit cells are kept in the mirror configuration as shown in Fig. 4 (b) and the RCS was simulated. In Configuration 6, all the unit cells of Configuration 5 were rotated by 180 deg. After comparing the RCS reduction characteristics of all the designs, Configuration 5 was found suitable for wideband Radar Cross Section reduction. The methods like superstrate loading<sup>23</sup> and co-planar loading can be used for integrating the metasurface with a patch antenna. In this design, co-planar loading of the metasurface is used. The integration is carried out in such a way that the mutual coupling of the PCM elements does not degrade the antenna radiation pattern.

#### 5. RESULTS AND DISCUSSION

The conventional patch antenna and the metasurface loaded microstrip patch antenna are simulated in CST Microwave Studio software. The resonant frequency of the

conventional antenna is 3.63 GHz. The modified antenna is resonating at the frequency of 3.6359 GHz which is almost the same as that of the conventional patch antenna. The top views of the fabricated antennas are shown in Fig. 5 (a) and Fig. 5 (b). The bottom views of the fabricated antennas are shown in Fig. 5 (c) and Fig. 5 (d). Fig. 5 (e) shows the simulated reflection coefficients of the Reference Patch Antenna and the Antenna with PCM. Fig. 5 (f) shows the experimentally measured reflection coefficient of the Antenna with PCM. The simulated reflection coefficient obtained is around -10.31 dB whereas the experimentally measured reflection coefficient is around -11.2 dB.

Figure 6 (a) compares the structural mode RCS reduction performance of all the four configurations with the Reference Patch Antenna having the same substrate dimensions. Fig. 6 (b) compares the simulated RCS values of the proposed patch antenna (Configuration 5), the reference patch antenna and the metal sheet of the same dimensions (70 mm × 70 mm). With

the proposed patch antenna, overall RCS reduction bandwidth of 3.49 GHz – 20 GHz (140.57%) can be obtained as compared with the metal sheet. At the frequency of 4.66 GHz and from 12 GHz – 14 GHz, RCS reduction is not significant but these short intervals can be neglected as far as theoretical RCS reduction bandwidth is considered.

In addition to this, 10 dB RCS reduction is obtained from 8.84 GHz - 10.45 GHz (16.41%) and from 16.99 GHz - 17.81 GHz (4.71%) as compared with the metal sheet. If the proposed antenna is compared with the conventional antenna then overall RCS reduction is obtained from 4.2196 GHz - 11.554 GHz (93%) and from 14.431 GHz - 19.647 GHz (30.61%). 10 dB RCS reduction is obtained from 8.835 GHz to 10.35 GHz (15.79%). The RCS reduction peaks are observed at 5.46 GHz, 9.1 GHz, 9.89 GHz and 17.41 GHz as shown in the simulation results. For the frequencies below 3 GHz, no significant cross-polarization conversion is obtained by the metasurface, so RCS reduction is not observed for these frequencies. The design

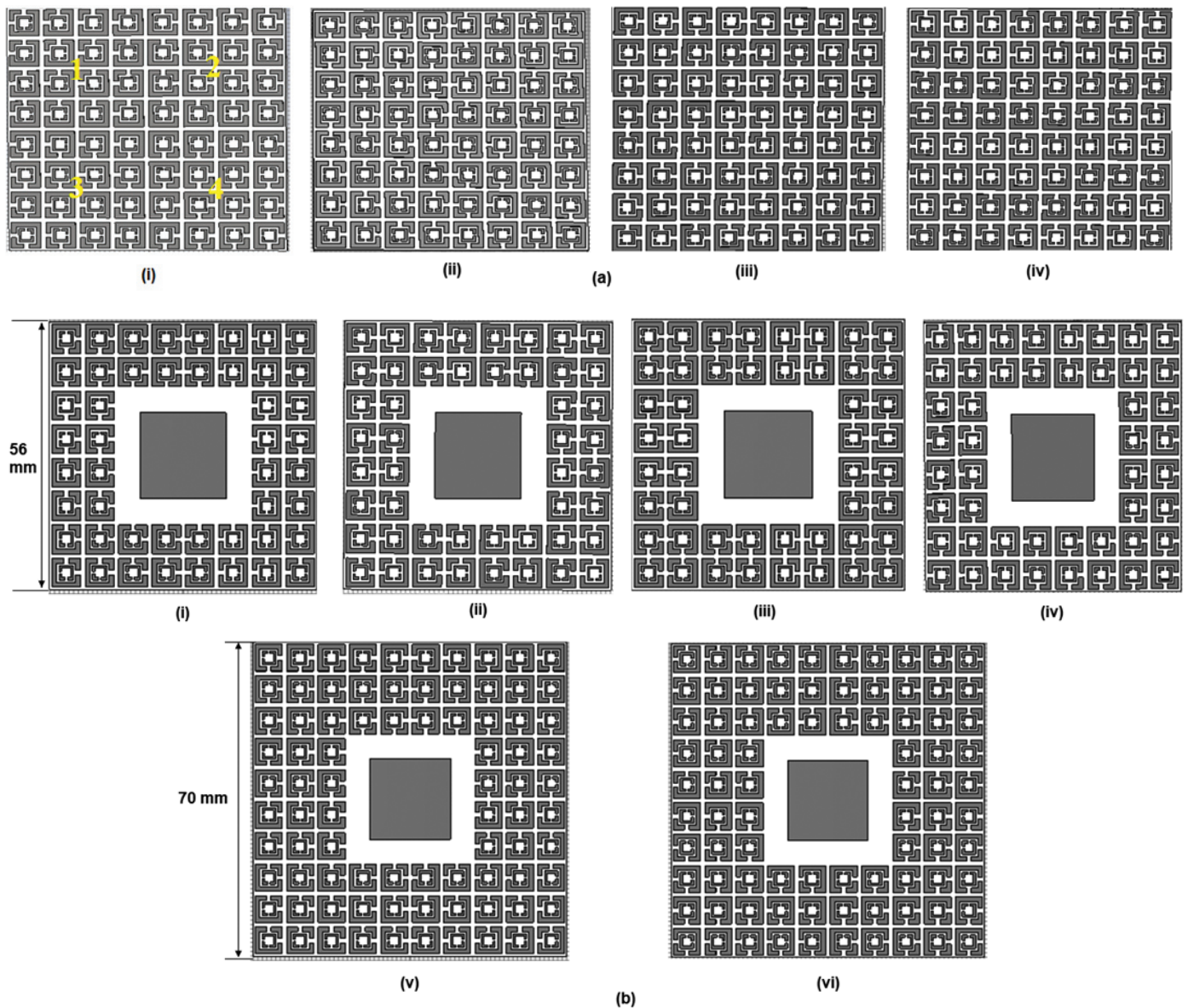


Figure 4. (a) Various configurations for the design of metasurface (b) various configurations for the evolution of the antenna design.

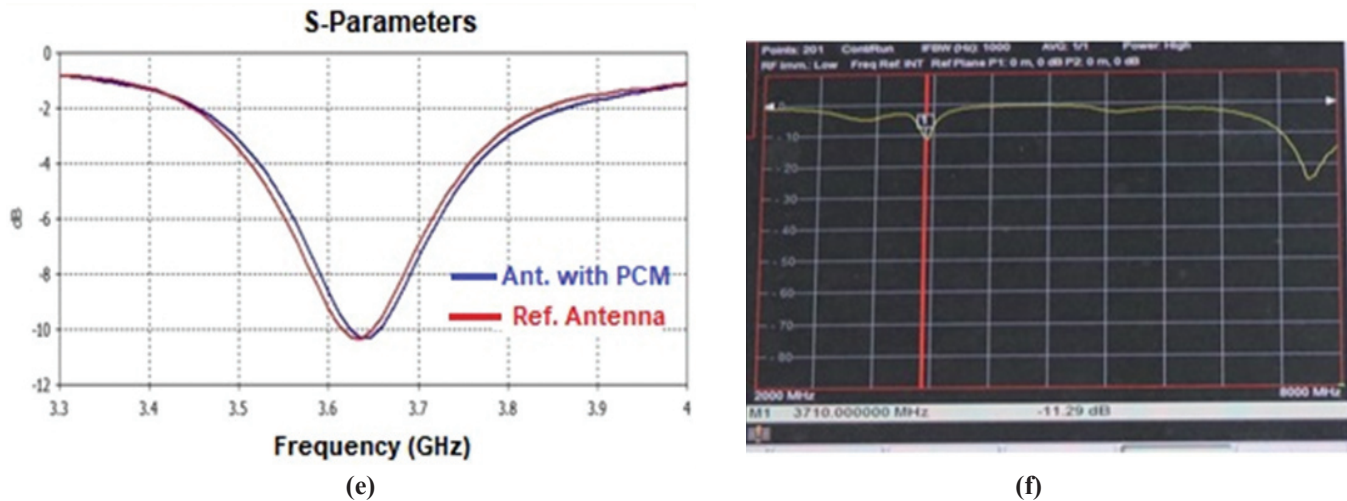
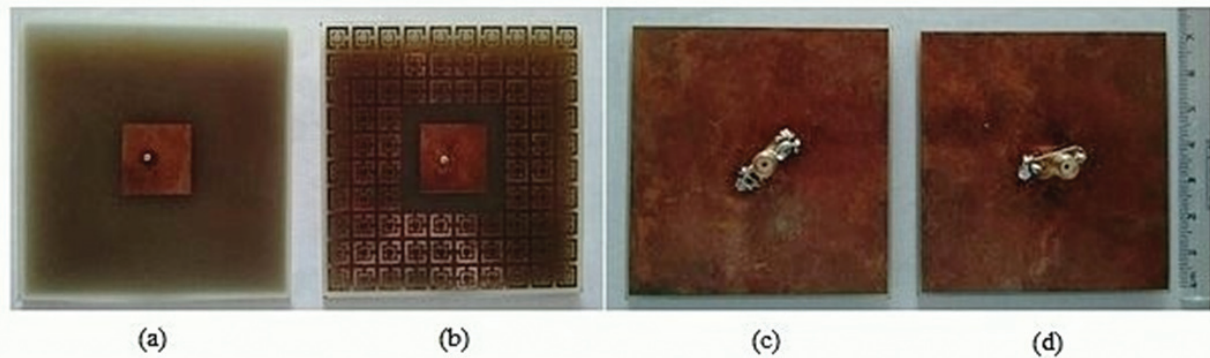


Figure 5. Fabricated patch antennas; (a) Top view of simple patch, (b) Top view of metasurface loaded patch antenna, (c) Bottom view of simple patch, (d) Bottom view of metasurface loaded patch antenna, (e) Simulated reflection coefficients of the reference patch and the antenna with PCM, and (f) Experimentally measured reflection coefficient of the patch antenna with PCM.

shows RCS reduction over S, C, X, Ku and the initial portion of K band as far as overall RCS reduction is considered. 10 dB RCS reduction can be observed for X-band, the succeeding portion of Ku-band and the initial portion of K-band. Special Airport Radars are used in S-band to locate the aircraft. Short and medium range radars can be used in C-band for military applications. X-band is used for CW radars, pulsed radars and Synthetic Aperture Radars. This band is used for defence tracking applications. For guided missile systems Ku band is used and for short range applications K band is used.

Figure 7 shows the inside view of the anechoic chamber in which the experimental measurements of RCS were carried out. Fig. 7(a) shows the transmitter and receiver horn antennas and Fig. 7(b) shows the calibration sphere. Fig. 7(c) and Fig. 7(d) show the experimental setup for radiation pattern measurements of both the antennas in the anechoic chamber. Fig. 7(e) shows the simulated RCS of the modified antenna for oblique incidence. The RCS values are evaluated at 0 deg., 10 deg. and 20 deg. angles of incidence. Because of the structural symmetry of the antenna, these values remain identical for TE mode as well as TM mode at the normal incidence. The simulated results show that in the case of oblique incidence, the peak RCS reduction frequencies remain nearly the same and better RCS reduction is achieved.

RCS measurements were performed in the anechoic chamber facility in the 3-18 GHz frequency range. Initially, the antenna was positioned on a low density transparent thermocol stand in the quiet zone of the anechoic chamber. The chamber was calibrated w.r.t. to a sphere of size 25.25 cm and bore sighting of antennas was carried out before the measurements. After completion of the calibration procedure, the test sample is placed in the anechoic chamber. A fully automated optimization procedure is used for bore-sighting the sample in Azimuth and Elevation directions, so as to orient it to normal to the incident waves. After the optimization procedure, the data acquisition of the measurement frequencies is carried out via control software. This raw data is processed to get the absolute RCS values in dBsm. Initially, the RCS of a metal plate mounted on a computer controlled turntable, is measured to obtain the reference RCS values. Thereafter, patch antenna and patch antenna with Polarization Converter Metasurface were measured. Measurements were performed in the time domain to identify the particular peak and then the data was transformed to the frequency domain.

Figure 8(a) compares experimentally measured RCS values of a metal plate of the same dimensions, patch antenna without metasurface and patch antenna with metasurface. It shows that the RCS values of the metal plate continuously increase with increasing frequency.

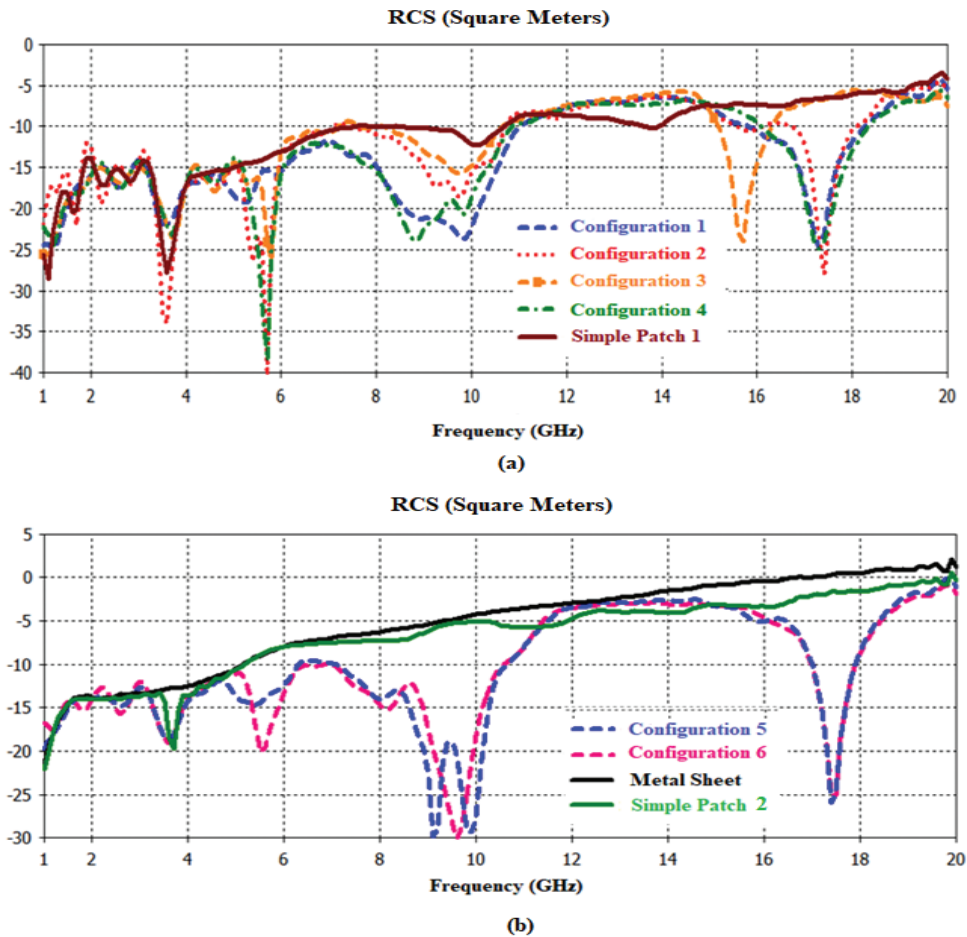


Figure 6. (a) RCS comparison of Config. 1, Config. 2, Config. 3 and Config. 4 and Ref. Patch 1, (b) RCS comparison of Config. 5, Config. 6, Metal Sheet and Ref. Patch 2.

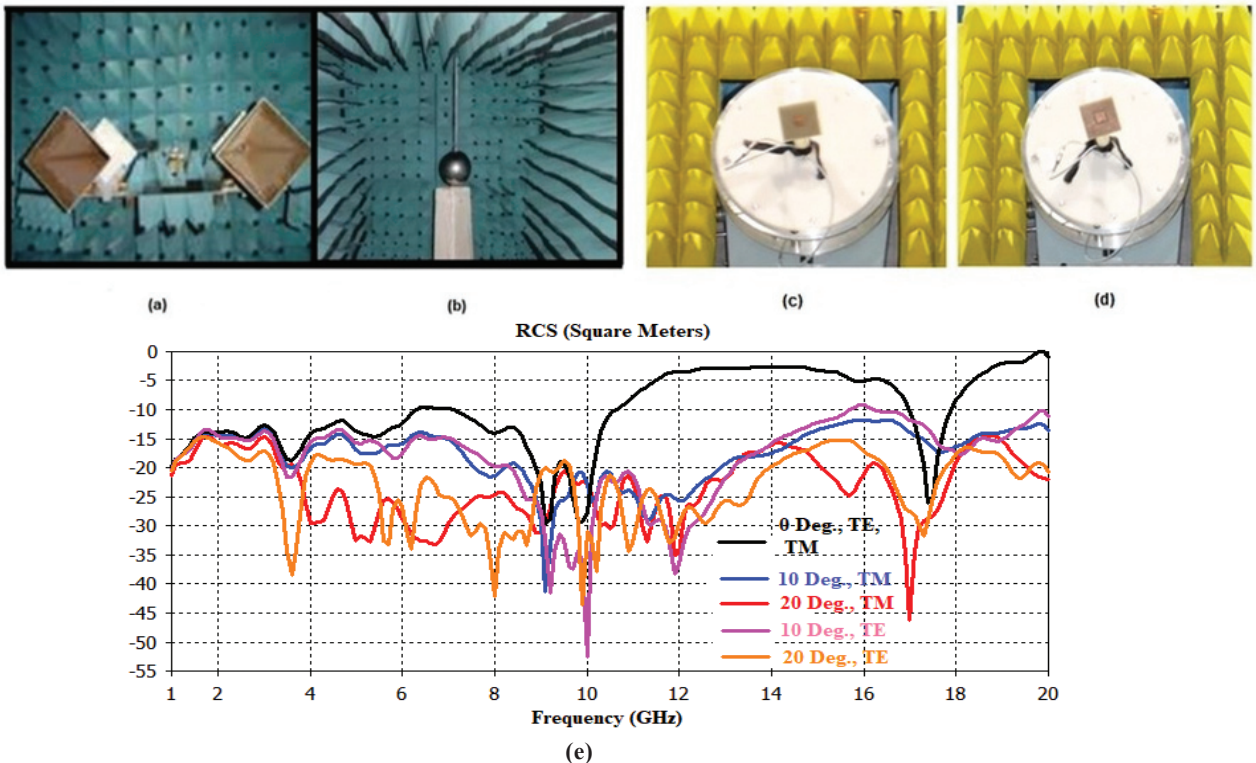


Figure 7. Inside view of the anechoic chamber; (a) Tx/Rx antenna assembly, (b) Calibration sphere, (c) Experimental setup to measure radiation pattern of the Ref. Patch, (d) Antenna with metasurface, (e) Simulated RCS of the antenna with PCM at oblique incidence for TE and TM modes.

If the conventional antenna is used, then it provides almost the same RCS values as those obtained by the metal plate. The patch antenna with metasurface provides significant RCS reduction. The metasurface loaded patch antenna provides RCS reduction peaks at 5.6 GHz, 9.1 GHz and 10.25 GHz frequency points. The RCS values at these frequencies are -18 dBsm, -37 dBsm and -38 dBsm respectively. The overall RCS reduction bandwidth is 4.7 GHz – 11 GHz and 14.5 GHz– 20 GHz as compared with the Reference Patch Antenna. The 10 dB RCS reduction is obtained from 8.8 GHz - 10.65 GHz. RCS reduction of the order of -10 dB is observed from 17.4 GHz - 17.814 GHz. Due to the limitations of the experimental measurement facility the results were verified up to 18 GHz. So, the simulated and measured results show good agreement. Slight differences may occur due to fabrication tolerances. Fig. 8 (b) shows measured values of RCS versus frequency for Horizontal Polarization as well as Vertical Polarization. Due to the structural symmetry, the RCS responses for both the polarizations remain the same. So, we can conclude that the structure provides RCS reduction for TE as well as TM polarization.

Fig. 9 (a) and Fig. 9 (b) show the simulated gain patterns of the conventional patch antenna in both the principal planes. At the resonance frequency, the peak gain value is 4.36 dB in the E-plane. Whereas, the peak gain value is 4.27 dB in the H-plane. Fig. 9 (c) and Fig. 9 (d) show the simulated gain patterns of the

patch antenna with metasurface in both the principal planes. It shows that the modified antenna has the peak gain value of 4.13 dB in the E-plane. The modified antenna shows the peak gain value of 4.02 dB in the H-plane. After observing the radiation diagrams of both the conventional antenna and the antenna with metasurface, it can be concluded that the metasurface loading does not degrade the antenna radiation parameters. The metasurface reduces the RCS of the antenna significantly.

Figure 9(e) and Fig. 9(f) show the experimentally measured radiation patterns of the Reference Antenna in both the principal planes. Whereas Fig. 9(g) and Fig. 9(h) show the measured radiation patterns of the Patch Antenna with Metasurface in both the principal planes. In experimental polar patterns, the main lobe is shown at 90 deg. due to the post-processing of the measurement software data. The experimental polar patterns are plotted from -90 deg. to +90 deg. because of the limitations of the positioner. The experimental results are in good agreement with the simulated results. The measured gain values in the boresight direction for the Reference Antenna are 3.9 dB in the E-plane and 3.85 dB in the H-plane. The measured gain values for the antenna with PCM are 4.1 dB and 3.55 dB in the E-plane and in the H-plane respectively. The gain is measured by the Friss-Transmission Method.

Figure 10(a) shows the 3D gain pattern of the conventional antenna and Fig. 10(b) shows the 3D

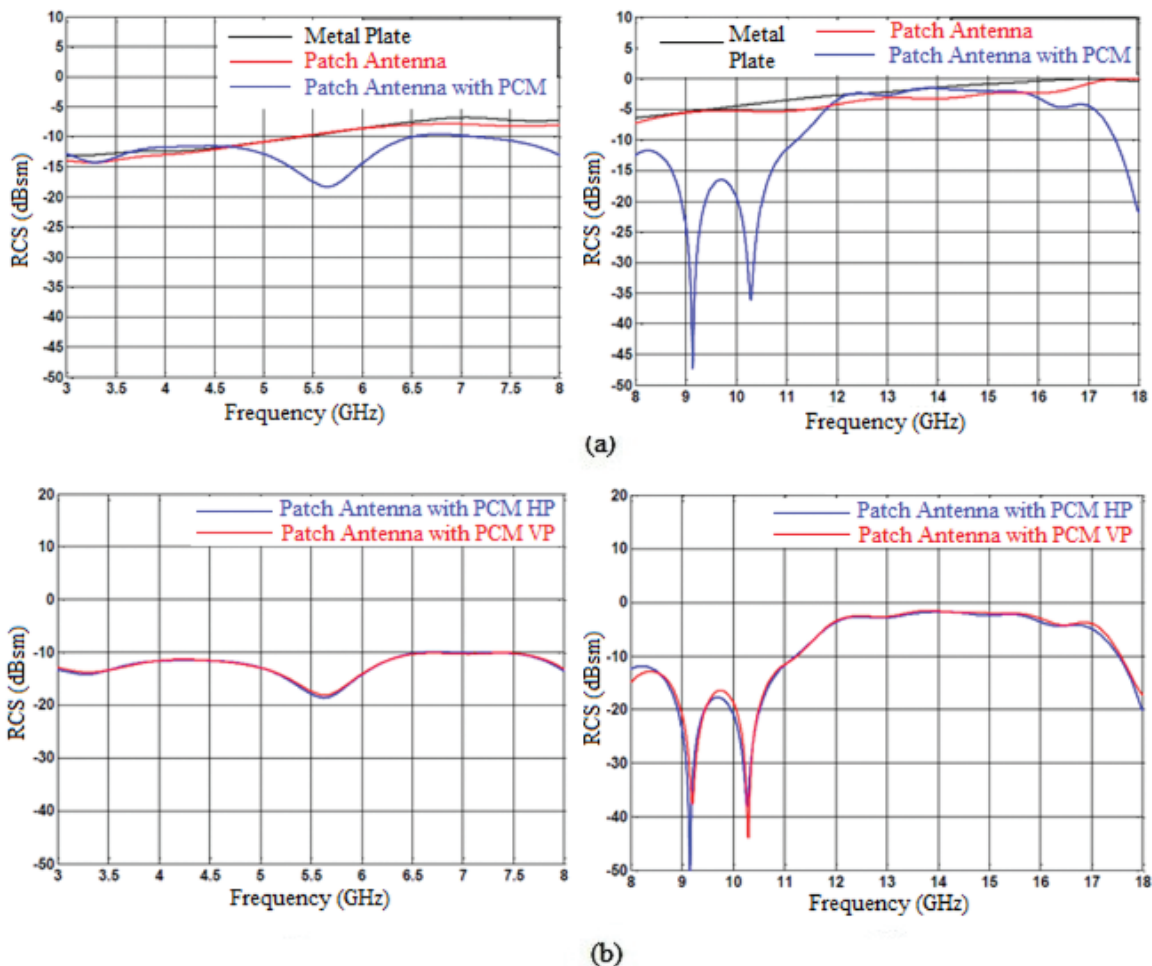


Figure 8. (a) Experimentally measured values of Radar Cross Section (RCS) from 3 GHz – 18 GHz (b) Experimentally measured RCS versus frequency response in HP and VP of patch antenna with metasurface from 3 GHz – 18 GHz.

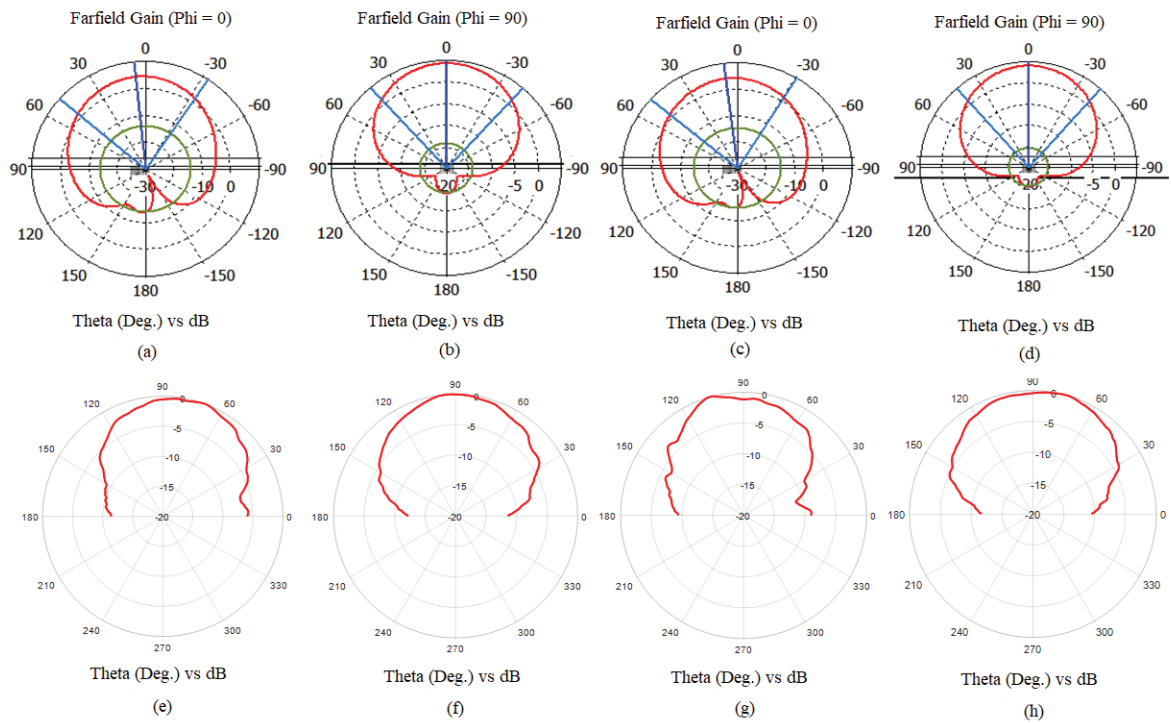


Figure 9. Simulated gain patterns of the conventional antenna in: (a) E-plane and (b) H-plane; Simulated gain patterns of the patch antenna with metasurface in (c) E-plane and (d) H-plane; Experimentally measured radiation patterns of the conventional antenna in (e)  $\phi = 0$  deg. plane and (f)  $\phi = 90$  deg. plane, Experimentally Measured Radiation patterns of the antenna with metasurface in (g)  $\phi = 0$  deg. plane and (h)  $\phi = 90$  deg. plane.

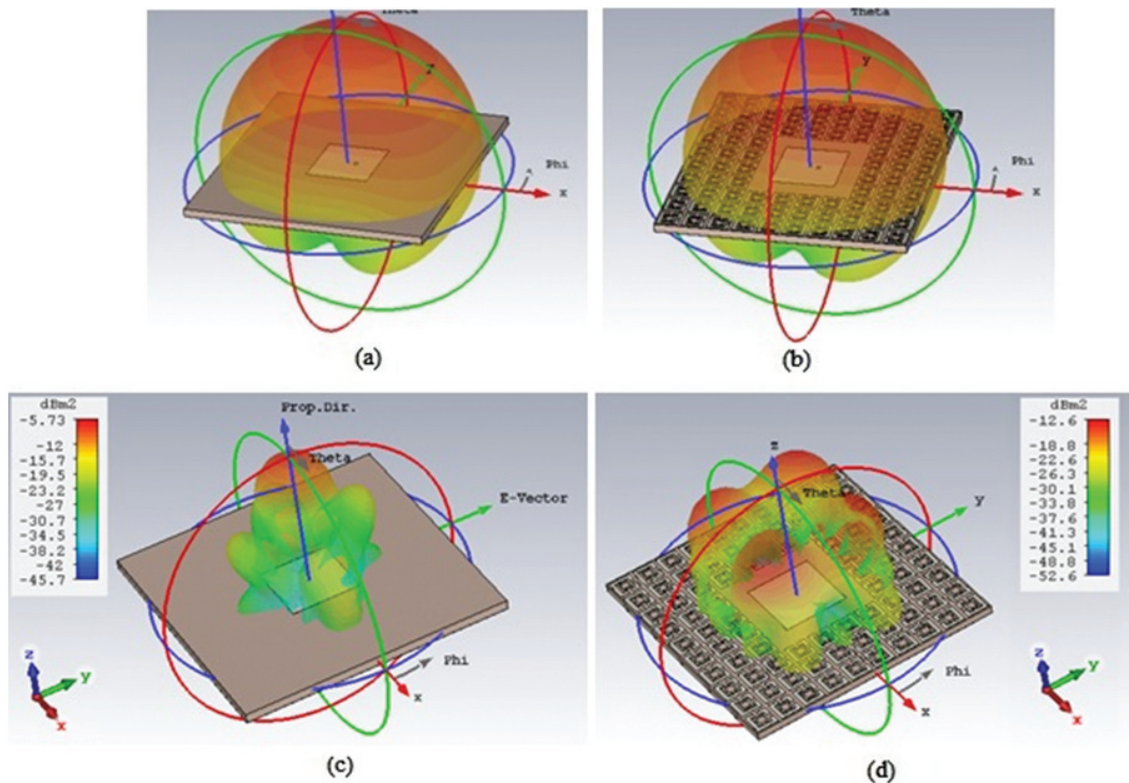


Figure 10. 3D Gain patterns of: (a) Conventional antenna, (b) Patch antenna with metasurface; bistatic scattering at 9.1 GHz for (c) Reference antenna, (d) Antenna with metasurface.

gain pattern of the modified antenna. The 3D gain patterns show that the radiation characteristics of the metasurface loaded patch antenna are not degraded.

Figure 10(c) and Fig. 10(d) show the bistatic scattering for the Reference Antenna and the Antenna with Metasurface respectively. The 3D scattering patterns show that in case of the Reference Antenna, the reflected field is in the boresight direction, whereas in case of the metasurface based antenna, the returned field is minimized in the boresight direction. It is scattered in various directions. With this design, Bistatic RCS reduction can also be achieved.

## 6. COMPARISON WITH SIMILAR WORK

Table 1 shows the comparison of the proposed design with the published work and shows its advantages over the existing state-of-the-art. The comparison is made in terms of RCS Reduction Bandwidth, Design Methodology,

reduction is obtained from 8.84 GHz - 10.45 GHz (16.41 %) and from 16.99 GHz - 17.81 GHz (4.71 %) as compared with the metal sheet. If the metasurface loaded antenna is compared with the conventional antenna then overall RCS reduction is obtained from 4.2196 GHz - 11.554 GHz (93 %) and from 14.431 GHz - 19.647 GHz (30.61%). 10 dB RCS reduction is obtained from 8.835 GHz - 10.35 GHz (15.79 %) and from 17.15 GHz - 17.75 GHz (3.44 %). It also shows excellent angular stability up to 70 deg. angle of incidence. Due to structural symmetry, the RCS reduction performance is similar for TE as well as TM polarizations. The simulated and measured results show that excellent out-of-band RCS reduction is obtained without degradation of the antenna radiation pattern. The Polarization Converter Metasurface shows superior performance as compared with Radar Absorbing Materials, Metamaterial Absorbers and other types of Frequency Selective Surfaces.

**Table 1. Comparison of the proposed design with similar work**

Reference, Year of Publication	Methodology Used	Limitations	Percentage Bandwidth	Design Complexity
[17], 2021	Polarization Converter Metasurface	Narrow Bandwidth, Angular stability was not discussed	15.5 GHz – 16.5 GHz (Linear to linear polarization conversion freq. range)	Not used for RCS reduction of antennas
[18], 2019	JC structure based on SRR	Narrow Bandwidth	absorption peaks at 8.6, 10.2, 11.95 GHz	Not integrated with patch
[19], 2016	Complimentary SRRs	No angular stability, Narrow bandwidth	RCS reduction peaks at 2.2 GHz and at 3.05 GHz	CSRRs in the ground plane
[13], 2016	Polarization Rotator	Not used for RCS reduction of a microstrip antenna	47.75 % (5.50-8.94 GHz) and 16.78 % ( 13.30-15.50 GHz)	Simple and feasible design
[12], 2013	Polarization Converters	No Polarization conversion for oblique incidence, Narrow BW	2-3.5 GHz (54.55%) (for Conversion Efficiency greater than 56%)	Not integrated with patch
Proposed Design	Polarization Converters	Excellent Angular Stability w.r.t various angles of incidence and polarization (TE as well as TM)	Overall RCS reduction BW(almost 3.49 – 20 GHz, 140.57% as compared with PEC), (4.2196 – 11.554 GHz, 93% and 14.431 – 19.647 GHz (30.61%) as compared with patch)	Single Layer Design, Co-planar integration of metasurface

Angular Stability, Radiation Pattern Degradation and Design Complexity. The comparison shows that the proposed design offers larger bandwidth for out-of-band RCS reduction, angular stability and no radiation pattern degradation as compared with other methodologies.

## 7. CONCLUSION

A novel patch antenna with Polarization Converter Metasurface is presented. The proposed design of the patch antenna shows excellent RCS reduction for a wide frequency range and it can be used on the low observable platforms. The overall RCS reduction bandwidth ranges almost from 3.49 GHz - 20 GHz (140.57 %) as compared with the metal sheet. 10 dB RCS

## ACKNOWLEDGEMENTS

The author is thankful to Dr Raghavan (Head) and Dr. R.K. Jani (Scientist E, MW-CAM) of Defence Research Development Organization (DRDO) for providing RCS measurement facilities. The author would like to thank Dr Milind Mahajan (Group Director, ASG), Mr. Sanjeev Kulshreshtha (Head, ATMD), Mr. K.P. Raja (Scientist G), Mr. Dharmendra Singh (Scientist D), Mr. Indra Prakash (Scientist C) and Mr. Priyanshu of Indian Space Research Organization (ISRO) for giving support in measurements like gain, reflection coefficient and providing the radiation pattern measurement facilities in the anechoic chamber.

**REFERENCES:**

1. Konstantinidis, K; Feresidis, A.P. & Hall, P.S. Broadband sub-wavelength profile high-gain antennas based on multi-layer metasurfaces. *IEEE Trans. Antennas Propag.*, 2015, **63**(1), 423-427. doi: 10.1109/TAP.2014.2365825.
2. Chen, L.; Lei, Z.; Yang, R.; Fan, J. & Shi, X. A broadband artificial material for gain enhancement of antipodal tapered slot antenna. *IEEE Trans. Antennas Propag.*, 2015, **63**(1), 395-400. doi: 10.1109/TAP.2014.2365044
3. Hao, Y.W.; Liu, Y.; Li, K. *et al.* Wideband radar cross-section reduction of microstrip patch antenna with splitting resonators. *Electronic Letters*, 2015, **51**(20), 1608-1609. doi: 10.1049/el.2015.1725
4. Liu, X.; Gao, J.; Cao, X. Y. *et al.* A high gain and low scattering waveguide slot antenna of artificial magnetic conductor octagonal ring arrangement. *Radioengineering*, 2016, **25**(1), 46-52. doi: 10.13164/re.2016.0046
5. Chen, H.; Zhou, P.; Chen, L.; Deng, L. Study on the properties of surface waves in coated RAM layers and monostatic RCS performances of the coated slab. *Prog. Electromagn. Res. M*, 2010, **1**, 123-135. doi: 10.2528/PIERM09122101
6. Tao, H.; Landy, N.I.; Bingham, C.M.; Zhang, X.; Averitt, R.D. & Padilla, W.J. A metamaterial absorber for the terahertz regime: Design, fabrication and characterization. *Optical Express*, 2008, **16**, 7181-7188. doi: 10.1364/OE.16.007181
7. Li, H.; Yuan, L.H.; Zhou, B.; Shen, X.P.; Cheng, Q. & Cui, T.J. Ultrathin multiband gigahertz metamaterial absorbers. *J. Appl. Phys.*, 2011, **110**, 014909. doi: 10.1063/1.3608246
8. Nguyen, T.T. & Lim, S. Angle and polarization insensitive broadband metamaterial absorber using resistive fan – shaped resonators. *Appl. Phys. Lett.*, 2018, **112**(2), 021605. doi: 10.1063/1.5004211
9. Yuan, F. *et al.* Broadband RCS reduction based on spiral-coded metasurface. *IEEE Antennas and Wireless Prop. Letters*, 2017, **16**, 3188-3191. doi: 10.1109/LAWP.2017.2768129
10. Jiang, W.; Xue, Y.; Gong, S.X. Polarization Conversion Metasurface for broadband Radar Cross Section reduction. *Prog. Electromagn. Res. Lett.*, 2016, **62**, 9-15. doi: 10.2528/PIERL16060504
11. Hong-Ya, C.; Jia-Fu, W.; Hua, M.; Shao-Bo, Q.; Jie-Qiu, Z.; Zhuo, X. & An-Xue, Z. Broadband perfect polarization conversion metasurfaces. *Chin. Phys. B.*, 2015, **24**(1), 014201. doi: 10.1088/1674-1056/24/1/014201
12. Feng, M.; Wang, J.; Ma, H.; Mo, W.; Ye, H.; Qu, S. Broadband polarization rotator based on multi-order plasmon resonances and high impedance surfaces. *J. Appl. Phys.*, 2013, **114**, 074508. doi: 10.1063/1.4819017
13. Yang, D.; Lin, H. & Huang, X. Dual Broadband Metamaterial Polarization Converter in microwave regime. *Prog. Electromagn. Res. Lett.*, 2016, **61**, 71-76. doi: 10.2528/PIERL16033004
14. Ali, S.; Davies, J.R.; Mendonca, J.T. Inverse Faraday effect with linearly polarized laser pulses. *Phys. Rev. Lett.*, 2010, **105**(3), 035001. doi: 10.1103/PhysRevLett.105.035001
15. Zhang, X. *et al.* Broadband terahertz wave deflection based on C-shape complex metamaterials with phase discontinuities. *Adv. Mater.*, 2013, **25**(33), 4567-4572. doi: 10.1002/adma.201204850
16. Qi, Y.; Zhang, B.; Liu, C. & Deng, X. Ultra-Broadband Polarization Conversion Meta-Surface and its application in polarization converter and RCS reduction. *IEEE Access*, 2020, **8**, 116675-116684. doi: 10.1109/ACCESS.2020.3004127
17. Pouyanfar, N.; Nourinia, J. & Ghobadi, C. Multiband and multifunctional polarization converter using an asymmetric metasurface. *Sci. Rep.*, 2021, **11**, 9306. doi: 10.1038/s41598-021-88771-x
18. Jafari, F.S.; Naderi, M.; Hatami, A.; Zarrabi, F.B. Microwave Jerusalem Cross absorber by metamaterial split ring resonator load to obtain polarization independence with triple band application. *AEU- International Journal of Electronics and Communications*, 2019, **101**, 138-144. doi: 10.1016/j.aeue.2019.02.002
19. Wang, S.; Chen, M.; Wang, J.; Zhang, Z.; Li, Z. & Li., Y. Radar cross section reduction of a microstrip antenna with CSRRs loaded on the ground. In 11th International Symposium on Antennas, Propagation and EM Theory (ISAPE), Guilin, China, 2016. pp. 670-673. doi: 10.1109/ISAPE.2016.7834043.
20. Yu, H.; Cao, X.; Gao, J.; Yang, H.; Jidi, L.; Han, J. & Li, T. Design of a wideband and reconfigurable polarization converter using a manipulable metasurface. *Opt. Mater. Express*, 2018, **8**, 3373-3381. doi: 10.1364/OME.8.003373.
21. Kumar, P.V.; Ghosh, B. Characteristic mode analysis of linear to circular polarization conversion metasurface. *Electromagnetics*, 2020, **40**(8), 605-612. doi: 10.1080/02726343.2020.1838058
22. Liu, X.; Gao, J.; Xu, L.; Cao, X.; Zhao, Y. & Li, S. A Coding Diffuse Metasurface for RCS reduction. *IEEE Antennas and Wireless Propagation Letters*, 2017, **16**, 724-727.
23. Zheng, Yue-Jun; Gao, Jun; Cao, Xiang-yu; Li, Si-jia & Li, Wen qiang. Wideband RCS reduction and gain enhancement microstrip antenna using chessboard configuration superstrate. *Microwave and Optical Technology Letters*, 2015, **57**(7), 1738-1741. doi: 10.1002/mop.29167
24. Costa, F.; Monorchio, A. & Manara, G. Wideband scattering diffusion by using diffraction of periodic surfaces and optimized unit cell geometries. *Sci. Rep.*, 2016, **6**, 25458. doi: 10.1038/srep25458
25. Munk, B.A. Frequency selective surfaces: Theory and design. Wiley, New York, 2000.
26. Shokati, E. & Granpateh, N. High operative polarization

converter using metasurface consisted of dual reciprocal L-shaped graphene array. *J. Nanophotonics*, 2020, **14**(1), 016015.

doi: 10.1117/1.JNP.14.016015

27. Luukkonen, O.; Costa, F.; Simovski, C.R.; Monorchio, A. & Tretyakov, S.A. A thin electromagnetic absorber for wide incidence angles and both polarizations. *IEEE Trans. Antennas Propag.*, 2009, **57**(10), 3119-3125.

doi: 10.1109/TAP.2009.2028601.

## CONTRIBUTORS

**Prof. Krunal Patel** has received his ME (Electronics and Telecommunication) degree from the University of Mumbai and BE (Electronics and Telecommunication) degree from North Maharashtra University in 2012 and 2008, respectively. Currently, he is pursuing PhD degree in Electronics and Telecommunication Engineering from

NMIMS University, Mumbai. He is also working as an Assistant Professor at Government Engineering College, Bhuj. His areas of interest include: Antenna Theory and Design and Microwave Engineering.

In this work, he has investigated the novel patch antenna loaded with polarization converter metasurface. He has used the simulation tools like CST Microwave Studio and Ansys HFSS to simulate the design. He has also verified the results experimentally.

**Dr Manjusha Joshi** is working as an Assistant Professor in the Department of Electronics and Telecommunication at Mukesh Patel School of Technology Management and Engineering, NMIMS University, Mumbai. She has more than 20 years of teaching experience. She has published more than 11 journal papers and 5 conference papers. Her areas of interest include: Antennas and Neural Networks.

She has worked as the PhD supervisor of the author.